Published in final edited form as:
Nat Struct Mol Biol. 2019 August 22; 26(10): 970–979. doi:10.1038/s41594-019-0307-x.

FACT mediates cohesin function on chromatin

Jonay Garcia-Luis[1], **Luciana Lazar-Stefanita**[2], **Pilar Gutierrez-Escribano**[1], **Agnes Thierry**[2], **Axel Cournac**[2], **Alicia García**[3], **Sara González**[3], **Mar Sánchez**[3], **Adam Jarmuz**[1], **Alex Montoya**[4], **Marian Dore**[5], **Holger Kramer**[4], **Mohammad Mehdi Karimi**[5], **Francisco Antequera**[3], **Romain Koszul**[2,*], **Luis Aragon**[1,*]

[1]Cell Cycle Group, MRC London Institute of Medical Sciences (LMS), Du Cane Road, London W12 0NN

[2]Institut Pasteur, Department Genomes and Genetics, Unité Régulation Spatiale des Génomes, Paris, France/ CNRS, UMR 3525, Paris, France

[3]Instituto de Biología Funcional y Genómica (IBFG), CSIC / Universidad de Salamanca, Zacarías González, nº 2, 37007 Salamanca, Spain

[4]Biological Mass Spectrometry and Proteomics Facility, MRC London Institute of Medical Sciences (LMS), Du Cane Road, London W12 0NN

[5]Bioinformatics Facility, MRC London Institute of Medical Sciences (LMS), Du Cane Road, London W12 0NN

Abstract

Cohesin is a regulator of genome architecture with roles in sister chromatid cohesion and chromosome compaction. The recruitment and mobility of cohesin complexes on DNA is restricted by nucleosomes. Here we show that the role of cohesin in chromosome organisation requires the histone chaperone FACT in *S. cerevisiae*. We find that FACT interacts directly with cohesin, and is dynamically required for its localization on chromatin. Depletion of FACT in

*Corresponding authors.

Reporting Summary
Further information on experimental design is available in the Nature Research Reporting Summary linked to this article.

Data Availability
ChIP-seq and MNase-seq data that support the findings of this study have been deposited in the GEO database and are accessible through the following accession number: GSE118534. Hi-C raw sequences are accessible via the SRA database through the following accession number: PRJNA486513. The mass spectrometry proteomics data have been deposited to the ProteomeXchange Consortium via the PRIDE partner repository with the dataset identifier PXD014896. Source data for Figure 1b, c, 3d, and 5 are available online. Any further data that support the findings of this study are available from the corresponding authors upon request

Author contributions
J. G-L. performed all yeast experiments providing samples for nucleosome mapping, HiC and sequencing. J. G-L. performed IP and cell biology experiments. L.L-S. and A.T. performed HiC experiments and analysis. A. C. analysed HiC data. A.G, S.G. M.S. performed and analysed nucleosome position experiments. M.D. and M.K. performed bioinformatic analysis. P. G-E. performed experiments related to the pulldowns for mass spectrometry and analysed result data. H.K. and A.M. performed technical mass spectrometry analysis. A.J. performed molecular biology experiments to generate constructs. J. G-L. and L.A. conceived the project. L.A. wrote the manuscript. L.A., F.A. and R.K. revised the manuscript.

Competing interests
The authors declare no competing interests.

Europe PMC Funders Author Manuscripts

metaphase cells prevents cohesin accumulation at pericentric regions and causes reduced binding on chromosome arms. Using Hi-C, we show that cohesin-dependent TAD (Topological Associated Domains)-like structures in G_1 and metaphase chromosomes are reduced in the absence of FACT. Sister chromatid cohesion is intact in FACT-depleted cells, although chromosome segregation failure is observed. Our data shows that FACT contributes to the formation of cohesin-dependent TADs thus uncovering a new role for this complex in nuclear organisation during interphase and mitotic chromosome folding.

Cohesin complexes not only hold sister chromatids but spatially organise chromosomes into loop domains [1–3]. Cohesin has been suggested to perform these functions by co-entrapment of DNAs within a tripartite ring [4]. Cohesin contains a pair of SMC proteins with ABC-like ATPase domains that are formed as the N and C terminal domains come into contact when the proteins fold onto themselves [5]. In addition, the interaction of the SMC pair through a folded hinge shapes them into a V structure that is subsequently bound by the N- and C-terminal domains of a kleisin subunit, generating a ring [4] thought to embrace DNAs. Until recently, the role of cohesin was thought to be in the maintenance of sister chromatid cohesion [5], however recent studies have demonstrated that the complex also modulates the organisation of interphase nuclei and mitotic chromosomes. [2,3,6]. Analysis of vertebrate cohesin has shown that it is required to fold individual chromatids into distinct loops by maintaining contacts between different loci in *cis* [6]. The current favoured model for how these cohesin-dependent loops might be formed on chromosomes involves capture and bending of a DNA segment by cohesin rings to form a loop that progressively becomes larger [7]. This activity is usually referred to as loop extrusion [7]. Direct evidence for cohesin loop extrusion activity has not yet been obtained. In contrast, single molecule analyses of a related SMC complex, condensin, has shown an ability to form DNA loops in a manner consistent with extrusion [8]. The activity of cohesin in loop extrusion was proposed to explain two main observations; that cohesin is required to maintain *cis* looping [6] and, that cohesin is blocked at TAD borders by CTCF on sites exhibiting convergent CTCF DNA motifs [7,9]. It is currently not clear whether cohesin can indeed extrude loops or it requires an associated DNA translocase to do so.

Single molecule analysis of purified cohesin complexes has shown a capacity to diffuse along naked λ-DNA molecules in an ATP-independent manner [10]. Interestingly, the presence of nucleosomes on these λ-DNA molecules was shown to restrict cohesin mobility [10]. In addition to blocking cohesin diffusion [10] nucleosomes have an inhibitory effect on cohesin binding. The ATP-dependent chromatin remodeler RSC (Remodels the Structure of Chromatin) and the Irc5 complex in yeast, as well as the SNF2 complex in humans are required for cohesin association to chromosomes [11–13]. Collectively, these findings suggest that cohesin functions on chromatinised eukaryotic genomes that involve binding to specific sites or translocation, require accessory factors to overcome nucleosomes. Here we set out to identify chromatin-remodelers that are important for cohesin function. We found that in addition to RSC, the histone chaperone FACT (Facilitates chromatin transcription) is a key regulator of cohesin's role in genome folding, but dispensable for its function in sister chromatid cohesion.

Results

Cohesin binding leads to changes in nucleosome positions at pericentric regions

We first sought to analyse if nucleosomal occupancy is dynamic at sites of cohesin binding. In *Saccharomyces cerevisiae CEN* sequences are cohesin loading sites where complexes initially access chromosomes before spreading towards pericentric regions [14–17]. Genome-wide MNase-seq maps were generated [18] in G_1 and G_2/M arrests to analyse nucleosome occupancy around centromeric regions (Fig. 1a). Although the yeast genome is characterised by having well-defined nucleosomal positions throughout [19], we detected differences in the positioning and occupancy of individual nucleosomes around pericentromeric regions between the G_1 and G_2/M MNase-seq maps (Fig. 1a). The general trend involved the loss of defined positioning in G_2/M arrests (increased nucleosome fuzziness- Fig 1b). The differences were confirmed using DANPOS 2 [20] (Fig. 1b) and showed a general correlation with regions enriched in pericentric cohesin (Fig. 1c). Moreover, auxin-mediated degradation of cohesin's kleisin Mcd1 in G_2/M arrests shifted the nucleosomal profiles closer to what we had observed for G_1 arrests (Fig. 1a), i.e. reverting nucleosome fuzziness (Fig. 1b). Together the results are consistent with the idea that nucleosomes are dynamic around *CEN* regions where cohesins are loaded and spread to pericentromeric sites.

The Cohesin complex physically interacts with chromatin remodellers

Next, we sought to identify potential chromatin remodellers involved in cohesin function. To this aim, cells expressing Mcd1 tagged with 6xHA were arrested in metaphase and Mcd1 immunoprecipitates were analysed by mass spectrometry (Table 1). Importantly, cell extracts were treated with benzonase to eliminate DNA prior to Mcd1 immunoprecipitation, to rule out indirect interactions mediated by DNA (Fig. 1d). We found that some chromatin remodellers were highly enriched in our pulldowns (Table 1). The most abundant was the Spt16 subunit of the FACT complex (facilitates chromatin transcription) (Table 1). Consistent with previous reports [21], several subunits of RSC were also amongst the hits (Table 1).

We were particularly intrigued by the identification of FACT because chromosome assembly *in vitro* requires FACT alongside the SMC complex condensin [22]. FACT is a heterodimeric complex containing Spt16 and Pob3 that acts as a histone chaperone regulating the assembly and disassembly of nucleosomes during transcription elongation, DNA replication and DNA repair [23]. The ability of FACT to mobilise nucleosomes makes it an ideal candidate to facilitate cohesin functions on chromatin or the extrusion of chromatin loops through cohesin rings. We confirmed the interaction between cohesin and FACT in metaphase arrests using cells that expressed *SMC1-6HA* and *SPT16-9MYC* to validate that cohesin physically interacts with this histone chaperone (Fig. 1e).

FACT is necessary for the localization of cohesin on yeast chromosomes

To further explore a possible functional relationship between FACT and cohesin, we sought to test whether inactivation of FACT in G_2/M arrests caused any alterations in cohesin binding. An auxin (IAA)-inducible degron of Spt16 (*SPT16-AID*) [24] was used to deplete FACT from cells in metaphase (Suppl. Fig. 1). We performed calibrated ChIP-seq as

described in the literature [25] for Smc1, a subunit of the cohesin complex, to analyse cohesin localisation before and after Spt16 depletion along yeast chromosomes (Fig. 2a). Centromeric regions are ideal sites to study cohesin translocation because cohesin complexes are initially loaded at core *CEN* sequences and then move away towards pericentromeric regions [17]. We observed a small effect on cohesin localisation to core *CEN* sequence upon Spt16 degradation, however its accumulation at pericentric regions was severely reduced (Fig. 2a-b). This suggest that FACT might not be required for cohesin initial loading at *CEN* sites [25], but it is necessary for its accumulation on peri-centric regions (Fig. 2b). Mcd1 is expressed at low levels in G_1-arrested cells, thus cohesin association to pericentric regions is very modest at this stage of the cell cycle [17]. However, cohesin loading can still occur in G_1 [25] when cohesin expression is artificially induced. Indeed, expression of *MCD1* from the *GAL1-10* promoter caused a significant enrichment of Smc1 both at core *CEN* sequences and the surrounding pericentric regions (Fig. 2c). In contrast, *MCD1* expression in G_1-arrests depleted in Spt16 showed no enrichment of cohesin at pericentric regions (Fig. 2c), despite the fact that Smc1 still was present at core *CEN* sequences (Fig. 2c). Therefore, these results demonstrate that in the absence of the histone chaperone FACT, cohesins can be loaded at core *CEN* sites but fail to accumulate at pericentric regions. To confirm that the loss of cohesin signal in FACT-depleted cells was not due to a defect in the ability of cohesin to load, we first tested whether cohesin loading occurs in G_2/M arrested cells (the stage where we depleted FACT in our experiments). To do this, we used an auxin (IAA)-inducible degron of Sth1 (*STH1-AID*), a core subunit of RSC, because RSC is required for cohesin loading[26]. Cohesin binding around centromeres and chromosome arms was similar to wildtype cells in the Sth1-depletion (Fig. 2d & Suppl. Fig. 2). In addition, FACT depletion in the absence of the cohesin release factor Wapl also did not affect cohesin binding on chromosomes (Fig. 2d), demonstrating that cohesin can be loaded normally in the absence of FACT. Therefore, the loss of cohesin signal in FACT-depleted cells cannot be caused by an impairment in cohesin loading but rather the stability of cohesin on chromatin.

FACT contribution to cohesin localization is independent of transcription

In yeast, cohesin complexes can be divided into two classes with respect to their chromosomal association mechanisms, those loaded at *CEN* sequences, which move and accumulate in pericentric regions [27,28], and those that load at chromosomal arm sites and translocate to regions of convergent transcription [29]. Importantly, the translocation of cohesins from *CEN* sites to pericentromeric regions requires Scc2 [17] and is independent of transcription [17], while the movement of arm loaded cohesins to sites between convergent genes involves relocation dependent on transcription [29–32]. FACT plays important roles during transcription initiation and elongation[33,34]. Therefore, we decided to investigate to what extent changes in transcription upon FACT-depletion are responsible for the disruption in the cohesin ChIP profiles. First, we focused on centromeric regions where transcription should not affect movement of *CEN* loaded cohesins to pericentric regions [17]. To confirm that accumulation of cohesin at pericentromeric regions does not require active transcription, we treated wildtype cells with the transcription repressor thiolutin and used calibrated ChiP-seq to Smc1 to compare cohesin enrichment in the presence and absence of active transcription (Fig. 3a). Thiolutin treatment had little effect on Smc1 binding at core *CEN* sequences or pericentric sites (Fig. 3a). Therefore, as reported previously[17], accumulation of

cohesin at these sites is independent of transcription. In contrast, Spt16 degradation in thiolutin-treated cells caused a reduction in cohesin presence on pericentric regions (Fig. 3a). Therefore, at pericentric regions FACT facilitates cohesin accumulation independently of active transcription.

The analysis of cohesin translocation on chromosome arms is more challenging that at centromeres because cohesin loading sites at chromosome arms are not well defined. ChIP profiles reflect the final position of the complexes. Our results demonstrate that FACT inactivation causes a decrease in cohesin binding at chromosomal arm sites (Fig. 2a). We therefore decided to test whether the effect of FACT on cohesin deposition at chromosome arms was independent on transcription, as observed for pericentric regions (Fig. 3a). Smc1 binding across chromosome arm sites was reduced in wildtype cells treated with thiolutin (Fig. 3b) confirming that active transcription is important for cohesin enrichment at these sites [29–32]. Thiolutin treatment in FACT-depleted cells caused a further reduction in cohesin binding across chromosome sites (Fig. 3b).

To further dissect the contribution of FACT to cohesin stability, we analysed how Smc1 enrichment at convergent transcription sites correlates with the changes in transcription at these sites when Spt16 is depleted (Fig. 3c). Analysis of cohesin binding sites confirmed their enrichment in positions in the genome where transcription units are oriented in a convergent manner [29–31]. Interestingly, cohesin enrichment was observed as a double peak at both 3’ ends of the genes (Fig. 3c). We classified convergent sites into categories depending on whether the transcription of the flanking genes had change by 2-fold up or down or had remain the same (Fig. 3c) upon Spt16 depletion. We then compared cohesin enrichment changes in each transcription-pair category (Fig. 3c). Smc1 was reduced similarly in all categories (Fig. 3c). Therefore, we conclude that FACT has a direct function in cohesin stability on chromosome arm sites and that changes in cohesin binding cannot be explained solely by the altered transcription profiles upon depletion of Spt16.

FACT is not required for sister chromatid cohesion

Having demonstrated that FACT has a role in maintaining cohesin on chromosomes (Fig. 3a-c), we sought to investigate the functional consequences for chromosome architecture. Cohesin holds sister chromatid together [35,36] and organises intra-chromatid loops that provide an integral level of structure to chromosomes [2,3]. First, we tested whether cohesion between sister chromatids is affected in G_2/M arrested cells when Spt16 is depleted. We scored cohesion using *tetO/tetR*-based tags at sub-telomeric regions of chromosome IV (Fig. 3d). Cells depleted for Spt16 showed no defects in cohesion (Fig. 3d).

FACT activity affects the role of cohesin in genome folding

Next, we tested whether Spt16 is necessary to maintain mitotic chromosome architecture. Recent studies on mitotic yeast chromosomes using Hi-C have shown that cohesin compacts chromosome arms through *cis* interactions, independently of sister chromatid cohesion [2,3]. We therefore considered the possibility that the reduction in cohesins observed upon Spt16-depletion (Fig. 2a) might impact on *cis* contacts along yeast metaphase chromosomes. To explore this, we built Hi-C libraries from G_2/M arrested cells depleted for Spt16 and

compared it to control arrests (Fig. 4a and Suppl. Fig. 3). The resulting contact maps show that depletion of Spt16 led to a reduction in short-distance intra-chromosomal contacts while long-range intra-chromosomal contacts were increased (> 100kb), as suggested by i) a larger width of the main diagonal in the contact maps of cells depleted for Spt16 (Suppl. Fig. 3), and as confirmed by computing ii) the contact probability p as a function of genomic distance s of all chromosome arms (Fig. 4b) and iii) the log-ratio between the normalized contact maps of depleted and non-depleted cells (Fig. 4a). The ratio map also shows that Spt16 depletion cause an increase of inter-chromosomal contacts (Fig. 4a). These results suggest that chromatin fibres loose internal organization in the absence of Spt16.

To further characterize mitotic chromosomes, 2 kb contact maps were generated. At this resolution, triangular contact patterns reminiscent of the topological associating domain (TADs) described in metazoans appear along mitotic chromosomes in G_2/M arrested cells but not G_1 arrests (Fig. 4c). The boundaries of these domains involve regions enriched in cohesin (red diamonds, Fig. 4c), and stronger contacts between pairs of boundaries are often visible, consistent with the establishment of cohesin loops (black triangles, Fig. 4c) (previous Hi-C studies on cohesin failed to directly characterize these loops, as the experiments were not analysed at this resolution [2,3]). We tested whether the triangular patterns of the 2 kb contact maps were dependent on cohesin. To this aim, we built Hi-C libraries from cells depleted for Mcd1 while arrested in G_2/M (Fig. 2c). The resulting contact maps showed a significant reduction in TAD-like structures (Fig. 4c), as expected from previous reports demonstrating a key role for cohesin in loop formation [2,3,6]. The depletion of Spt16 results in a strong reduction of cohesin deposition (Fig. 4c), as well as a fading of the cohesin-dependent TADs-like domains signal (Fig. 4c).

Our Hi-C analysis is consistent with a role for FACT in affecting cohesin-dependent loops, however we cannot differentiate whether FACT is important to establish these loops or to maintain them. To test a potential role for FACT in *de novo* loop formation by cohesin, we first investigated whether overexpressing *MCD1* in G_1, which causes cohesin loading (Fig. 2c), leads to *de novo* formation of loop, which are normally absent in G_1 cells [2,3] (Fig. 4c). Hi-C libraries from G_1 arrested cells overexpressing Mcd1 from the *GAL1-10* promoter were thus generated. TADs-like domain signals were observed in 2 kb contact maps of G_1 overexpressing Mcd1 (Fig. 4d) demonstrating *de novo* loop formation by cohesin under this experimental condition (Fig. 4d). Next, we depleted Spt16 during the overexpression of Mcd1 in G_1 cells, cohesin dependent loops were now strongly reduced, and hardly visible, in the absence of FACT (Suppl. Fig. 4). The log-ratio between the normalized contact maps of G_1 depleted and non-depleted cells (Fig. 4e) and the contact probabilities as a function of genomic distance s of all chromosome arms (Fig. 4f) confirms that *de novo* loop formation by cohesins in G_1 requires FACT.

FACT-dependent chromosome organisation in metaphase is required for chromosome segregation

Our results demonstrate that while cohesin's role in sister chromatid cohesion is maintained in the absence of FACT (Fig. 3d), its function in organising chromatin loops in metaphase chromosomes is impaired (Fig. 4a-c). We therefore hypothesized that depletion of FACT in

metaphase arrested cells might lead to defects in chromosome structure that are likely to compromise the ability of chromosomes to segregate faithfully if allowed to proceed into anaphase. To test this, we arrested *SPT16-AID* cells in metaphase, depleted FACT, and released cells from the arrest. To ensure that cells did not pass beyond telophase, so that we could accurately score chromosome segregation, we performed these experiments in a *CDC15-AID* genetic background. Therefore, upon release from metaphase, the addition of auxin to degrade Spt16, also induced the degradation of the mitotic exit kinase Cdc15, causing a tight telophase arrest. Similar to our analysis of sister chromatid cohesion, we used *tetO/tetR*-based tags on chromosome IV to evaluate chromosome segregation in the Cdc15 block. As predicted, we observed high levels of chromosome missegregation in cells depleted for Spt16 and Cdc15, but not Cdc15 only (Fig. 5).

Discussion

In this study we identified FACT as a new regulator of cohesin in budding yeast. Our findings shed new light on the relationship between cohesin and chromatin factors and suggests a novel role of this histone chaperone in genome and chromosome organisation. FACT is a conserved histone chaperone, involved in both assembly and disassembly of core nucleosome particles by modulation of H2A-H2B histone dimers [37]. In yeast, FACT is a heterodimeric complex composed of Spt16 and Pob3 [38]. In addition, the HMG protein, Nhp6, is also required for FACT roles during transcription, replication and DNA repair [38]. Interestingly the ATP-dependent chromatin remodeling enzyme Chd1 (chromodomain-helicase-DNA binding protein 1) functions alongside FACT during transcription elongation [39]. Chd1 is a regulator of cohesin's roles in sister chromatid cohesion and chromosome condensation [40]. Interestingly, Chd1 was identified in our mass spectrometry screen as one of the chromatin factors physically interacting with Mcd1 (Table 1), raising the possibility that Chd1 regulation of cohesin is through FACT.

One of the prominent roles of FACT is in facilitating DNA replication[38], because nucleosome represent barriers for the unwinding of the MCM helicase. A direct interaction between MCM and FACT is thought to recruit the histone chaperone during replication and unfold DNA from histone octamers so that MCM movement can proceed through the chromatinised genome [41]. Our findings demonstrate that the movement of cohesin from its loading site at the core *CEN* sequence to the flanking pericentromeric regions is severely disrupted when FACT is depleted from yeast cells (Fig. 2b-c). This strongly suggests a role for FACT in facilitating cohesin movement through chromatin, at least at centromeric regions. It is also possible that FACT impacts on the loading of cohesin by binding to nucleosomes (particularly H2A-H2B dimers) and releasing free DNA that could then promote cohesin binding. Such a role would be similar to that described for RSC, which generates nucleosome-free regions allowing cohesin and its loader to access DNA [26]. It is however important to note that depleting FACT in the absence of Wapl supresses the loss of cohesin binding (Fig. 2d) observed when FACT is inactivated in wildtype cells (Fig. 2a). Therefore FACT is not strictly required for the loading of cohesin. Supporting this view is the observation that depletion FACT leads to very different effects on the localisation of bound cohesin compared to the inactivation of RSC; severe disruption in cohesin localisation is observed when FACT is inactivated in G2/M cells (Fig. 2a), while RSC depletion does not

affect the localisation of already bound cohesin (Fig. 2d). Therefore, it is likely that RSC plays a prominent role at the loading stage while FACT is required to maintain the stability of loaded cohesin on chromatin, either by facilitating its movement through nucleosomal arrays and/or counteracting its removal by anti-establishment factors, such as Wapl.

The translocation of cohesins from *CEN* sites to pericentromeric regions is independent of transcription [17]. However, cohesin is found on intergenic regions (IGRs) that lie between convergent genes[29–32] suggesting that its movement to these sites might be facilitated by transcription [29–32]. Since FACT is important during transcription initiation and elongation[33,34], an alteration of the transcription profile in FACT-depleted cells could impact on the changes observed in cohesin stability (Fig. 2a). Several lines of evidence rule out this possibility. First, when FACT is depleted in the absence of transcription, cohesin localisation is still disrupted (Fig. 3b). Second, like FACT-depletion, inactivation of RSC also alters transcription profiles, however stability of cohesin is not affected by RSC-depletion (Fig. 2d). These findings strongly suggest that the stability of bound cohesin in G2/M cells is not affected by transcription changes. We propose that transcription might play a more important role in the initial localisation of cohesin when they are loaded in S phase, but not in metaphase arrested cells.

Abrogating cohesin function leads to a loss of *cis*-loops required for TADs in interphase nuclei of human cells [6] as well as correct folding of mitotic chromosome arms in budding yeast [3]. Previous studies in yeast had not found structures resembling topologically associated domains (TADs) found in metazoans. However, when we increased the resolution of normalized contact maps to 2kb (Fig. 4a) we detected triangular contact patterns in mitotic chromosomes (G_2/M arrests) (Fig. 4a) which are comparable to the TAD structures described in metazoans. These structures were not observed in G1 (Fig. 4a), however overexpression of the kleisin subunit of cohesin in these G1 arrests led to the formation of *de novo cis*-looping and TAD-like structures (Fig. 4d) with similar characteristics to the structures observed in metaphase (Fig. 4a). This confirms that cohesin dependent loops can be formed in the absence of sister-chromatid cohesion [3], and demonstrates that cohesin role in genome folding is functionally distinct from its role in sister chromatid cohesion. Importantly, formation of G1 loops also required Spt16 (Fig. 4d), demonstrating that the cohesin-dependent process that leads to the formation or maintenance of these genomic structures heavily relies on the histone chaperone FACT.

In summary, our work demonstrates that the FACT complex is a mediator of cohesin stability on chromatin (Fig. 2b-c) and through this function facilitates the formation of cohesin-dependent loops (Fig. 4). Recently, an involvement of FACT in chromatin architecture independent of transcription has been proposed [42], our data suggests that this function might be related to cohesin's role in genome architecture. We speculate that similar to its roles in transcription and replication, FACT function as a histone chaperone is likely to occur through destabilization of core nucleosomal particles, to allow movement of cohesin on chromatin. We demonstrate that FACT contributes to cohesin's role in organizing mitotic chromosome folding but not sister chromatid cohesion. Finally, our results support the original claim that cohesin complexes have two distinct roles, in chromosome organisation

and sister chromatid cohesion [3543] and demonstrate that FACT is exclusively necessary for functions in genome folding.

Methods

Media, culture conditions and synchronisations

S. cerevisiae strains used in this study are shown in Supplementary Table 1. To arrest the cells in G1, α-factor was added to exponentially growing MATa cultures (OD600=0.5) to a final concentration of 3 x 10-8 M. To arrest cells in G2/M, Nocodazole (1.5 mg/ml stock in DMSO 100%) was added to exponentially growing cultures (OD600=0.5) to a final concentration of 0.015 mg/ml. When arrests in Nocodazole are maintained for more than 2 hours cells are spun and resuspended in YPD containing fresh nocodazole (0.015 mg/ml). Cultures were monitored by microscopy until ≥90% of cells were arrested, typically 2 hours at 25 °C. To release cells from G1, the culture was spun (4,000 r.p.m, 1 min) and washed in YPD 3 times. The pellet was then resuspended in YPD containing 0.1 mg/ml pronase. To release cells from Nocodazole, the culture was spun (4,000 r.p.m, 1 min) and washed in YPD containing 1% DMSO 5 times. The pellet was then resuspended in YPD. To degrade proteins tagged with AID* epitope, a stock of IAA of 0.6M in ethanol 100% was used for a final concentration of 6mM. To inhibit transcription a stock of thiolutin at 1mg/ml in DMSO was added for 30 minutes to the culture at a final concentration of 10ug/ml.

Microscopy

A Leica IRB epifluorescence microscope with a Hamamatsu 742-95 digital camera, a 63X/1.4 lens and OpenLab software (Improvision) was used for single cell visualization. 1 ml of cell culture was collected from each time point and mixed with glycerol (20% final concentration) to preserve TetO/TetR signal. Cells were then frozen at -80 °C. For visualization, cells where centrifuged at 3,000 r.p.m. for 2 minute and 1µl of the pellet was mixed with 1µl of DAPI solution (DAPI 4 µg/ml Triton 1 %) on the microscope slide. For each field 20 z-focal planes images were captured (0.3 µm depth between each consecutive image). At least 100 cells were score for GFP dots.

Hi-C libraries

Hi-C experiments were performed according to a protocol adapted from [44]. Aliquots of 1-3 x 10^9 cells in 150 ml culture medium were fixed in 3% formaldehyde (Sigma-Aldrich, Ref. F8775) and quenched in 0.4 M glycine for 20 min at room temperature and 4°C, respectively. Cells were harvested, washed with culture medium and pellets were stored at -80°C. Pellets were thawed on ice and resuspended in chilled TE buffer supplemented with protease inhibitors. Cells were lysed using Precellys VK05 Lysing KIT (Ozyme, Ref. 0042) at 6,700 rpm. Lysates were treated with 0.5 % SDS for 20 min at 65°C and digested overnight with DpnII (CFinal=500 U/pellet; NEB R0543M) at 37°C. Digestions were centrifuged for 20 min at 16,000 g and the pellets suspended in cold water. 5’ DpnII overhangs were filled-in and labelled with biotin using 30 µM dNTP (dATP, dGTP, dTTP and Biotin-14-dCTP Invitrogen Ref. 19518018). Biotinylated DNA fragments were ligated using T4 DNA ligase (CFinal=250 Weiss U/pellet; Thermo Scientific 10621441) for 4 h at 16°C. Cross-link was reverted through an overnight treatment in presence of 250 µg/ml

proteinase K at 65°C. Total DNA was extracted using phenol/chloroform, precipitated and treated with RNAse A 500 µg/ml. Non-ligated DNA fragments were removed by T4 DNA polymerase (CFinal=5 U/pellet; NEB M0203L) treatment; whereas ligated fragments were 500 bp sheared using Covaris S220 and pulled-down using Dynabeads Myone Streptavidin C1 (Invitrogen 65001). Resulting libraries were amplified using custom-made primers for paired-end deep-sequencing on NextSeq500 Illumina platform (2x75 bp cycles).

Generation and normalization of contact maps

The reads from each Hi-C library were processed as follows. First, PCR duplicates were removed using the custom-made tags present on the primers and the resulting reads were mapped independently using Bowtie 2 (mode: --very-sensitive --rdg 500,3 --rfg 500,3) against the reference genome of S. cerevisiae (S288C) and indexed on DpnII restriction fragments. An iterative alignment procedure (20 bp window) was used to maximize the yield of uniquely mapped reads (mapping quality > 30). Reads were classified as either valid Hi-C products or unwanted events to be filtered out (i.e. loops, non-digested fragments, etc.; for details see {Cournac, 2012 #40}) based on their assignment and orientation on the DpnII restriction fragments in the reference genome. Valid Hi-C reads were used to generate contact frequency maps. In these maps, each vector consists in a fixed size genomic bin made of successive RF (either 5, 25, or 50 kb). Bins with a high variance in contact frequency (< 1.5 Standard Deviation or 1.5 - 2 S.D.) were filtered out. Filtered contact maps were normalized as described [45]. Approximately 15 million of valid reads were used to build each contact map. Similarity between pairs of normalized contact maps was assessed by computing the log2 ratio for each point.

Contact probability as a function of the genomic distance p(s)

The contact probability p(s) as a function of the genomic distance s separating two DNA positions in cis was computed as follow. First, self-circularization events were discarded by removing pairs of read oriented in opposite directions along the reference genome and separated by less than 1.5 kb. The remaining reads were log-binned as a function of their genomic distance (in kb) on each chromosomal arm: bin = [log1.1(s)]. The p(s) curve is the histogram computed on the sum of read pairs for each bin. This sum is weighted by both bin-size $1.1^{(1+bin)}$ (log binning), as well as by the length of the chromosomes.

Chromatin immunoprecipitation

For ChIP analysis cells were grown to OD_{600} = 0.5 and arrested at the required cell cycle stage. 87 OD_{600} units of *S. cerevisiae* were mixed with 43 OD_{600} units of asynchronous *C. glabrata*. Cells were fixed for 15 minutes at 25 °C, and quenched with glycine (final concentration 125 mM) for 7 minutes before cells were harvested by centrifugation at 4,000 r.p.m. for 1 minute. The cell pellets were washed in PBS and transferred to a screw cap tube and frozen on dry ice. The pellets were stored at -80 °C. Pellets were resuspended in 300 µl of IP buffer (150 mM NaCl, 50 mM Tris-HCl (pH 7.5), 5 mM EDTA, NP-40 (0.05% v/v), Triton® X-100 (1% v/v)) containing phenylmethanesulfonyl fluoride (PMSF, final concentration 1 mM) and Complete protease inhibitor cocktail (without EDTA, from Roche). 500 µl of glass beads were added to the tubes. Cells were broken in a FastPrep® FP120 (BIO101) by 3 repetitions of a 20 seconds cycle, power setting 5.5. Cells were

maintained on ice for 2 minutes after each cycle. The tubes were pierced with a hot needle and placed into new eppendorf and spun at 2000 r.p.m. for 2 minutes to collect the lysate. 100 µl of IP buffer containing PMSF and protease inhibitors were then added and tubes spun again at 2000 r.p.m. for 1 minute. The cell lysate was spun down for 10 minutes at 15,000 r.p.m at 4 °C. This pellet was resuspended in 1ml of IP buffer containing PMSF and protease inhibitors, and sonicated for 1 hour (30 seconds on, 30 seconds off) at high power at 4 °C in a Diagenode Bioruptor. After sonication samples were spun down for 10 minutes at 15,000 r.p.m. and the supernatant taken. 200 µl of the sonicated chromatin were taken as "input" and 400 µl was incubated with 40 µg of HA antibody (anti-HA 12CA5 from Roche) in a sonicator at low power for 30 minutes (30 seconds on, 30 seconds off). The "input" DNA was precipitated with 0.3 M sodium acetate and 2.5 volumes of cold ethanol and spun down at 15,000 r.p.m. for 30 minutes, and the supernatant removed. The pellet was washed with 70 % ethanol and air dried. After antibody binding the IP sample was spun down at 13,000 r.p.m for 5 minutes and the supernatant added to 60 µl of Dynabeads protein G (Invitrogen) previously equilibrated with IP buffer. Then the samples were incubated for 2 hours at 4 °C in a rotating wheel and washed 5 times with IP buffer using a magnetic separator rack. Finally "input" samples and IP samples were resuspended in de-crosslinking buffer (TE 1X, 1 % SDS, 10 µg/ml RNase A, 1 mg/ml proteinase K) and incubated at 65 °C overnight. Samples were purified using ChIP DNA Clean & Concentrator kit (Zymoresearch) according to the manufacturer instructions.

Protein coimmunoprecipitation

Cells were grown to OD_{600} = 1 wash in cold water and resuspended in ice-cold buffer (50 mM HEPES, 150 mM KCl, 1.5 mM MgCl2, 0.5 mM DTT, and 0.5% Triton X-100 (pH 7.5) supplemented with Complete protease inhibitor cocktail tablets (from Roche)). Cells were broken in a FastPrep® FP120 (BIO101) by 3 repetitions of a 20 seconds cycle, power setting 5.5. Extracts were maintained on ice for 2 minutes after each cycle. To the cell extract 0.5mM $CaCl_2$, 20 U DnaseI (NEB), 0.2 mg RNaseA (Qiagen) and 500 U Benzonase (Millipore) were added in order to degrade DNA and RNA from the sample. Cell extracts were incubated with protein G Dynabeads (Invitrogen) bound to anti-Myc antibody (Roche, 9E10) for 2 h at 4°C. Finally, beads were washed 5 time in washing buffer (10mM Tris-Cl pH 7.5, 150mM NaCl, 0.5 % Triton) and unbound from the antibody by incubating at °C for 4 minutes in SR Buffer (2% SDS, 0.125 M Tris-Cl pH 6.8). Immunoprecipitated proteins were mixed with SS buffer (5% sacarose, 0.0125 % Bromophenol blue) and run in SDS-PAGE gel.

Digestion with MNase

Mononucleosomal DNA was prepared as described in [18]. For MNase digestions 160 ml of cells (OD600=1) where fixed with 1 % formaldehyde for 30 minutes at 25 °C with 100 r.p.m. agitation and quenched with 125 mM glycine for 10 minutes at 25 °C with 100 r.p.m. agitation. Cells were spun and washed twice with PBS. Pellet was resuspended in 20 ml sorbitol/ tris buffer (1M sorbitol, 50 mM Tris-HCl pH 7.5, 10 mM β-mercaptoethanol) containing 10 mg of Zymolyase 20T and incubated at 30 °C for 5 minutes or until spheroplast were formed. Spheroplasts were spun at 3,000 r.p.m. for 5 minutes and washed with sorbitol/tris buffer without β-mercaptoethanol. Spheroplasts were resuspended in NP

buffer (1 M sorbitol, 50 mM NaCl, 10mM Tris pH 7.5, 5 mM MgCl2, 1mM CaCl2, 1mM β-mercaptoethanol, 500 μM spermidine, 0.075 % NP40) and digested with 600, 1200 or 1800 U/ ml of MNase (NEB) for 20 minutes at 37 °C. MNase digestion was stopped adding 200 μl of STOP solution (5% SDS, 50 mM EDTA). DNA was decrosslinked by adding 1 mg/ml proteinase K and incubating at 65 °C overnight. DNA was purified by adding 0.6M potassium acetate pH 5.5 and incubating on ice 5 minutes and centrifuging 10 minutes at 3,500 r.p.m followed by a phenol chloroform extraction. Finally DNA was precipitated by adding 25 μg/ml glycogen, 1/25 columes NaCl, 0.7 volumes Isopropanol, incubating 30 minutes at -20 °C and centrifuging 30 minutes at 13,200 r.p.m. The pellet was washed in 70 % ethanol and resuspended in TE 1X. Samples were run in parallel in a 1.5 % agarose gel and the mononucleosomes of a digestion with a ratio of 80:20 mononucleosomes to dinucleosomes were purified and used in Next Generation Sequencing.

Next-generation sequencing and DANPOS analysis

Libraries of mononucleosomal and ChIP DNA were constructed following the Illumina compatible NEXTflexTM ChIP-Seq kit protocol and sequenced in an Illumina NextSeq500 platform using the paired-end protocol. Reads were aligned to the S.cerevisiae (SacCer3) genome using Bowtie [46]. Nucleosome occupancy maps were generated using the NUCwave algorithm [47]. Nucleosome fuzziness was analyzed using the dpos utility of DANPOS2 application [20]. To make it compatible with NUCwave maps, we used the following parameters: a span of 1 bp and a read extension of 50 bp. ChIP-seq data representation was performed using the Model-based Analysis of ChIP-Seq (MACS) [48] with a read extension of 147 bp.

Calibrated ChIP-Seq analysis

Calibrated Chip-seq analysis as done as in [25]. The quality of the raw sequence data was assessed using FastQC (version 0.11.5). The reads were mapped to the *S. cerevisiae* genome (sacCer3) as the experimental genome or *C. glabrata* genome (CBS138) as calibration genome using Bowtie2 (version 2.3.4) with the default parameters. To generate an alignment in which all the sequences exclusively map to the sacCer3 genome, the whole reads were first mapped to CBS138 genome and the unmapped reads were retrieved as a separate Fastq file. Subsequently, these unmapped reads were re-aligned to sacCer3 genome and the generated aligned BAM file therefore contained reads that were unique to sacCer3. The same method was used to generate alignments unique to CBS138.

Applying a recent published method [26] for calibrating ChIP-seq data and adding cells with the calibration genome (CBS138) to different samples of cells with the experimental genome (sacCer3), we calculated occupancy ratio (ORi) for experimental sample i from the number of reads assigned to calibration (WCi) and experimental (WXi) genomes among sequences derived from input DNA and the number of reads assigned to calibration (IPCi) and experimental (IPXi) genomes among sequences derived from ChIP-seq sample. Then ORi was calculated as:

$$ORi = \frac{Wci}{Wxi} \times \frac{IPxi}{IPci}$$

Europe PMC Funders Author Manuscripts

For each sample, the alignment BAM file was converted to Wig format using bedtools (version 2.27.1). To obtain a calibrated version, the Wig file with the conventional ChIP-seq profile was multiplied by the occupancy ratio (OR) corresponding to each sample. Subsequently, these calibrated BigWig files were used to generate average profile plots for regions in +/- 20KB of centromeres for 16 chromosomes in sacCer3 genome

All sequencing data that support the findings of this study have been deposited in GEO and are accessible through the following accession number: GSE118534.

MNase-seq data analysis

Paired-end Sequencing reads were aligned to Yeast genome sacCer3 using bowtie version 2.2.9 with default parameters. DANPOS2 was applied for two separate pair-wise comparisons at each nucleosome between G1 arrest and G2/M arrest, and G2/M arrest and G2/M +IAA. DANPOS output for pair-wise comparison contains a set of reference positions (with fixed length of 200bp) for nucleosomes defined by integrating all the nucleosomal positions called in each of the two conditions under study. The DANPOS-generated reference positions in two pair-wise comparisons were very similar but there was a small fraction of positions that did not overlap well in two comparisons. DANPOS also calculated Fuzziness scores for each condition and FDR and log10 p-value for each pair-wise comparison. We reported the nucleosomes with significant fuzziness change as reference nucleosomes in each comparison with FDR < 0.01 and p-value<-2, recommended in DANPOS manual. The fuzziness of these nucleosomes may be increased or decreased from one condition to the other. We also used DNAPOS-generated wig files for visualization of Fuzziness on IGV genome browser.

Mcd1 Pulldowns

MCD1-HA and MCD1 untagged strains expressing CDC20 under the galactose promoter were grown at 25ºC in YEP medium containing 2% galactose to mid-logarithmic phase and arrested in metaphase by the addition of 2% glucose. 800 ODs of cells were harvested at 4ºC, washed once with ice-cold water and frozen at -80ºC. Cell pellets were mechanically broken in Lysis Buffer containing 150 mM KCl, 1mM MgCl2, 0.12mM Cacl2 50 mM Tris pH 7, 1 mM EDTA, 1% Triton 100-X, 5% glycerol and 1 mM PMSF supplemented with EDTA-free Complete Protease Inhibitor and Phosphatase Inhibitor Cocktail tablets (Roche). Protein extracts were treated with 600μg of RNase A (Qiagen), 900U of Benzonase (Millipore) and 600U of DnaseI (NEB) and immunoprecipitated using anti-HA Epitope Tag Protein Isolation kit (Miltenyi Biotec). After 1h incubation at 4ºC, anti-HA magnetic beads were washed with 750mM NaCl-Lysis Buffer and subjected to 2 consecutive rounds of elution in 50mM Tris-HCl pH6.8, 5mM EDTA, 1%SDS and 50mM DTT elution buffer.

Protein identification and quantification by LC-MS/MS

Sample processing—Protein samples eluted from anti-HA magnetic beads were buffer exchanged, reduced and alkylated using a FASP protocol. Briefly, samples were loaded onto 30 kDa centrifugal concentrators (Millipore, MRCF0R030) and buffer exchange was carried out by centrifugation on a bench top centrifuge (15min, 12,000g). Multiple buffer exchanges were performed sequentially with UA buffer (8M urea in 100mM Tris pH 8.5, 3x200μl),

reduction with 10mM DTT in UA buffer (30min, 40°C) and alkylation with 50mM chloroacetamide in UA buffer (20min, 25°C). This was followed by buffer exchange into UA buffer (3x100µl) and 50mM ammonium bicarbonate (3x100µl). Digestion was carried out with mass spectrometry grade trypsin (Promega, V5280) using 1µg protease per digest (16h, 37°C). Tryptic peptides were collected by centrifugation into a fresh collection tube (10min, 12,000g) and washing of the concentrator with 0.5M sodium chloride (50µl, 10min, 12,000g) for maximal recovery. Following acidification with 1% trifluoroacetic acid (TFA) to a final concentration of 0.2%, collected protein digests were desalted using Glygen C18 spin tips (Glygen Corp, TT2C18.96) and peptides eluted with 60% acetonitrile, 0.1% formic acid (FA). Eluents were then dried using vacuum centrifugation.

Liquid chromatography-tandem mass spectrometry (LC-MS/MS) analysis— Dried tryptic digests were redissolved in 0.1% TFA by shaking (1200rpm) for 30min and sonication on an ultrasonic water bath for 10min, followed by centrifugation (20,000g, 5°C) for 10min. LC-MS/MS analysis was carried out in technical duplicates and separation was performed using an Ultimate 3000 RSLC nano liquid chromatography system (Thermo Scientific) coupled to a coupled to a Q-Exactive mass spectrometer (Thermo Scientific) via an EASY spray source (Thermo Scientific). For LC-MS/MS analysis protein digest solutions were injected and loaded onto a trap column (Acclaim PepMap 100 C18, 100µm × 2cm) for desalting and concentration at 8µL/min in 2% acetonitrile, 0.1% TFA. Peptides were then eluted on-line to an analytical column (Acclaim Pepmap RSLC C18, 75µm × 50cm) at a flow rate of 250nL/min. Peptides were separated using a 120 minute gradient, 4-25% of buffer B for 90 minutes followed by 25-45% buffer B for another 30 minutes (composition of buffer B – 80% acetonitrile, 0.1% FA) and subsequent column conditioning and equilibration. Eluted peptides were analysed by the mass spectrometer operating in positive polarity using a data-dependent acquisition mode. Ions for fragmentation were determined from an initial MS1 survey scan at 70,000 resolution, followed by HCD (Higher Energy Collision Induced Dissociation) of the top 12 most abundant ions at 17,500 resolution. MS1 and MS2 scan AGC targets were set to 3e6 and 5e4 for maximum injection times of 50ms and 50ms respectively. A survey scan m/z range of 400 – 1800 was used, normalised collision energy set to 27%, charge exclusion enabled with unassigned and +1 charge states rejected and a minimal AGC target of 1e3.

Raw data processing—Data was processed using the MaxQuant software platform (v1.5.8.3), with database searches carried out by the in-built Andromeda search engine against the Uniprot S.cerevisiae database (version 20160815, number of entries: 6,729). A reverse decoy search approach was used at a 1% false discovery rate (FDR) for both peptide spectrum matches and protein groups. Search parameters included: maximum missed cleavages set to 2, fixed modification of cysteine carbamidomethylation and variable modifications of methionine oxidation, protein N-terminal acetylation and serine, threonine, tyrosine phosphorylation. Label-free quantification was enabled with an LFQ minimum ratio count of 2. ‘Match between runs’ function was used with match and alignment time limits of 1 and 20 minutes respectively.

Europe PMC Funders Author Manuscripts

Supplementary Material

Refer to Web version on PubMed Central for supplementary material.

Acknowledgements

We thank the members of the L.A, R.K. and P.A. laboratories for fruitful discussions and advice. The work in the L.A. laboratory was supported by Wellcome Trust Senior Investigator award to L.A. (100955, “Functional dissection of mitotic chromatin”) and the “London Institute of Medical Research (LMS), which receives its core funding from the UK Medical Research Council. This research was further supported by funding from The European Research Council (R.K.), Agence Nationale pour la Recherche (R.K.) and the the Spanish Ministerio de Economía, Industria y Competitividad (BFU2017-89622-P) (F.A.).

References

1. Haarhuis JHI, et al. The Cohesin Release Factor WAPL Restricts Chromatin Loop Extension. Cell. 2017; 169:693–707 e14. [PubMed: 28475897]
2. Lazar-Stefanita L, et al. Cohesins and condensins orchestrate the 4D dynamics of yeast chromosomes during the cell cycle. EMBO J. 2017; 36:2684–2697. [PubMed: 28729434]
3. Schalbetter SA, et al. SMC complexes differentially compact mitotic chromosomes according to genomic context. Nat Cell Biol. 2017; 19:1071–1080. [PubMed: 28825700]
4. Haering CH, Lowe J, Hochwagen A, Nasmyth K. Molecular architecture of SMC proteins and the yeast cohesin complex. Mol Cell. 2002; 9:773–88. [PubMed: 11983169]
5. Nasmyth K. Disseminating the genome: joining, resolving, and separating sister chromatids during mitosis and meiosis. Annu Rev Genet. 2001; 35:673–745. [PubMed: 11700297]
6. Rao SSP, et al. Cohesin Loss Eliminates All Loop Domains. Cell. 2017; 171:305–320 e24. [PubMed: 28985562]
7. Fudenberg G, et al. Formation of Chromosomal Domains by Loop Extrusion. Cell Rep. 2016; 15:2038–49. [PubMed: 27210764]
8. Ganji M, et al. Real-time imaging of DNA loop extrusion by condensin. Science. 2018; 360:102–105. [PubMed: 29472443]
9. Rao SS, et al. A 3D map of the human genome at kilobase resolution reveals principles of chromatin looping. Cell. 2014; 159:1665–80. [PubMed: 25497547]
10. Stigler J, Camdere GO, Koshland DE, Greene EC. Single-Molecule Imaging Reveals a Collapsed Conformational State for DNA-Bound Cohesin. Cell Rep. 2016; 15:988–998. [PubMed: 27117417]
11. Huang J, Hsu JM, Laurent BC. The RSC nucleosome-remodeling complex is required for Cohesin's association with chromosome arms. Mol Cell. 2004; 13:739–50. [PubMed: 15023343]
12. Litwin I, Bakowski T, Maciaszczyk-Dziubinska E, Wysocki R. The LSH/HELLS homolog Irc5 contributes to cohesin association with chromatin in yeast. Nucleic Acids Res. 2017; 45:6404–6416. [PubMed: 28383696]
13. Hakimi MA, et al. A chromatin remodelling complex that loads cohesin onto human chromosomes. Nature. 2002; 418:994–8. [PubMed: 12198550]
14. Megee PC, Mistrot C, Guacci V, Koshland D. The centromeric sister chromatid cohesion site directs Mcd1p binding to adjacent sequences. Mol Cell. 1999; 4:445–50. [PubMed: 10518226]
15. Blat Y, Kleckner N. Cohesins bind to preferential sites along yeast chromosome III, with differential regulation along arms versus the centric region. Cell. 1999; 98:249–59. [PubMed: 10428036]
16. Tanaka T, Cosma MP, Wirth K, Nasmyth K. Identification of cohesin association sites at centromeres and along chromosome arms. Cell. 1999; 98:847–58. [PubMed: 10499801]
17. Petela NJ, et al. Scc2 Is a Potent Activator of Cohesin's ATPase that Promotes Loading by Binding Scc1 without Pds5. Mol Cell. 2018; 70:1134–1148 e7. [PubMed: 29932904]
18. Gonzalez S, et al. Nucleosomal signatures impose nucleosome positioning in coding and noncoding sequences in the genome. Genome Res. 2016; 26:1532–1543. [PubMed: 27662899]

19. Yuan GC, et al. Genome-scale identification of nucleosome positions in S. cerevisiae. Science. 2005; 309:626–30. [PubMed: 15961632]
20. Chen K, et al. DANPOS: dynamic analysis of nucleosome position and occupancy by sequencing. Genome Res. 2013; 23:341–51. [PubMed: 23193179]
21. Oum JH, et al. RSC facilitates Rad59-dependent homologous recombination between sister chromatids by promoting cohesin loading at DNA double-strand breaks. Mol Cell Biol. 2011; 31:3924–37. [PubMed: 21807899]
22. Shintomi K, Takahashi TS, Hirano T. Reconstitution of mitotic chromatids with a minimum set of purified factors. Nat Cell Biol. 2015; 17:1014–23. [PubMed: 26075356]
23. Formosa T. The role of FACT in making and breaking nucleosomes. Biochim Biophys Acta. 2013; 1819:247–55. [PubMed: 24459727]
24. Nishimura K, Kanemaki MT. Rapid Depletion of Budding Yeast Proteins via the Fusion of an Auxin-Inducible Degron (AID). Curr Protoc Cell Biol. 2014; 64:20 9 1–16.
25. Hu B, et al. Biological chromodynamics: a general method for measuring protein occupancy across the genome by calibrating ChIP-seq. Nucleic Acids Res. 2015; 43:e132. [PubMed: 26130708]
26. Lopez-Serra L, Kelly G, Patel H, Stewart A, Uhlmann F. The Scc2-Scc4 complex acts in sister chromatid cohesion and transcriptional regulation by maintaining nucleosome-free regions. Nat Genet. 2014; 46:1147–51. [PubMed: 25173104]
27. Fernius J, Marston AL. Establishment of cohesion at the pericentromere by the Ctf19 kinetochore subcomplex and the replication fork-associated factor, Csm3. PLoS Genet. 2009; 5:e1000629. [PubMed: 19730685]
28. Hu B, et al. ATP hydrolysis is required for relocating cohesin from sites occupied by its Scc2/4 loading complex. Curr Biol. 2011; 21:12–24. [PubMed: 21185190]
29. Lengronne A, et al. Cohesin relocation from sites of chromosomal loading to places of convergent transcription. Nature. 2004; 430:573–8. [PubMed: 15229615]
30. Glynn EF, et al. Genome-wide mapping of the cohesin complex in the yeast Saccharomyces cerevisiae. PLoS Biol. 2004; 2:E259. [PubMed: 15309048]
31. Gullerova M, Proudfoot NJ. Cohesin complex promotes transcriptional termination between convergent genes in S. pombe. Cell. 2008; 132:983–95. [PubMed: 18358811]
32. Busslinger GA, et al. Cohesin is positioned in mammalian genomes by transcription, CTCF and Wapl. Nature. 2017; 544:503–507. [PubMed: 28424523]
33. Formosa T. The role of FACT in making and breaking nucleosomes. Biochim Biophys Acta. 2012; 1819:247–55. [PubMed: 21807128]
34. Saunders A, et al. Tracking FACT and the RNA polymerase II elongation complex through chromatin in vivo. Science. 2003; 301:1094–6. [PubMed: 12934007]
35. Guacci V, Koshland D, Strunnikov A. A direct link between sister chromatid cohesion and chromosome condensation revealed through the analysis of MCD1 in S. cerevisiae. Cell. 1997; 91:47–57. [PubMed: 9335334]
36. Michaelis C, Ciosk R, Nasmyth K. Cohesins: chromosomal proteins that prevent premature separation of sister chromatids. Cell. 1997; 91:35–45. [PubMed: 9335333]
37. Kemble DJ, McCullough LL, Whitby FG, Formosa T, Hill CP. FACT Disrupts Nucleosome Structure by Binding H2A-H2B with Conserved Peptide Motifs. Mol Cell. 2015; 60:294–306. [PubMed: 26455391]
38. Bondarenko MT, et al. [Structure and function of histone chaperone FACT]. Mol Biol (Mosk). 2015; 49:891–904. [PubMed: 26710768]
39. Simic R, et al. Chromatin remodeling protein Chd1 interacts with transcription elongation factors and localizes to transcribed genes. EMBO J. 2003; 22:1846–56. [PubMed: 12682017]
40. Boginya A, Detroja R, Matityahu A, Frenkel-Morgenstern M, Onn I. The chromatin remodeler Chd1 regulates cohesin in budding yeast and humans. Sci Rep. 2019; 9:8929. [PubMed: 31222142]
41. Tan BC, Chien CT, Hirose S, Lee SC. Functional cooperation between FACT and MCM helicase facilitates initiation of chromatin DNA replication. EMBO J. 2006; 25:3975–85. [PubMed: 16902406]

42. McCullough LL, et al. Establishment and Maintenance of Chromatin Architecture Are Promoted Independent of Transcription by the Histone Chaperone FACT and H3-K56 Acetylation in Saccharomyces cerevisiae. Genetics. 2019

43. Heidinger-Pauli JM, Mert O, Davenport C, Guacci V, Koshland D. Systematic reduction of cohesin differentially affects chromosome segregation, condensation, and DNA repair. Curr Biol. 2010; 20:957–63. [PubMed: 20451387]

44. Belton JM, et al. Hi-C: a comprehensive technique to capture the conformation of genomes. Methods. 2012; 58:268–76. [PubMed: 22652625]

45. Cournac A, Marie-Nelly H, Marbouty M, Koszul R, Mozziconacci J. Normalization of a chromosomal contact map. BMC Genomics. 2012; 13:436. [PubMed: 22935139]

46. Langmead B, Salzberg SL. Fast gapped-read alignment with Bowtie 2. Nat Methods. 2012; 9:357–9. [PubMed: 22388286]

47. Quintales L, Vazquez E, Antequera F. Comparative analysis of methods for genome-wide nucleosome cartography. Brief Bioinform. 2015; 16:576–87. [PubMed: 25296770]

48. Zhang Y, et al. Model-based analysis of ChIP-Seq (MACS). Genome Biol. 2008; 9:R137. [PubMed: 18798982]

Europe PMC Funders Author Manuscripts

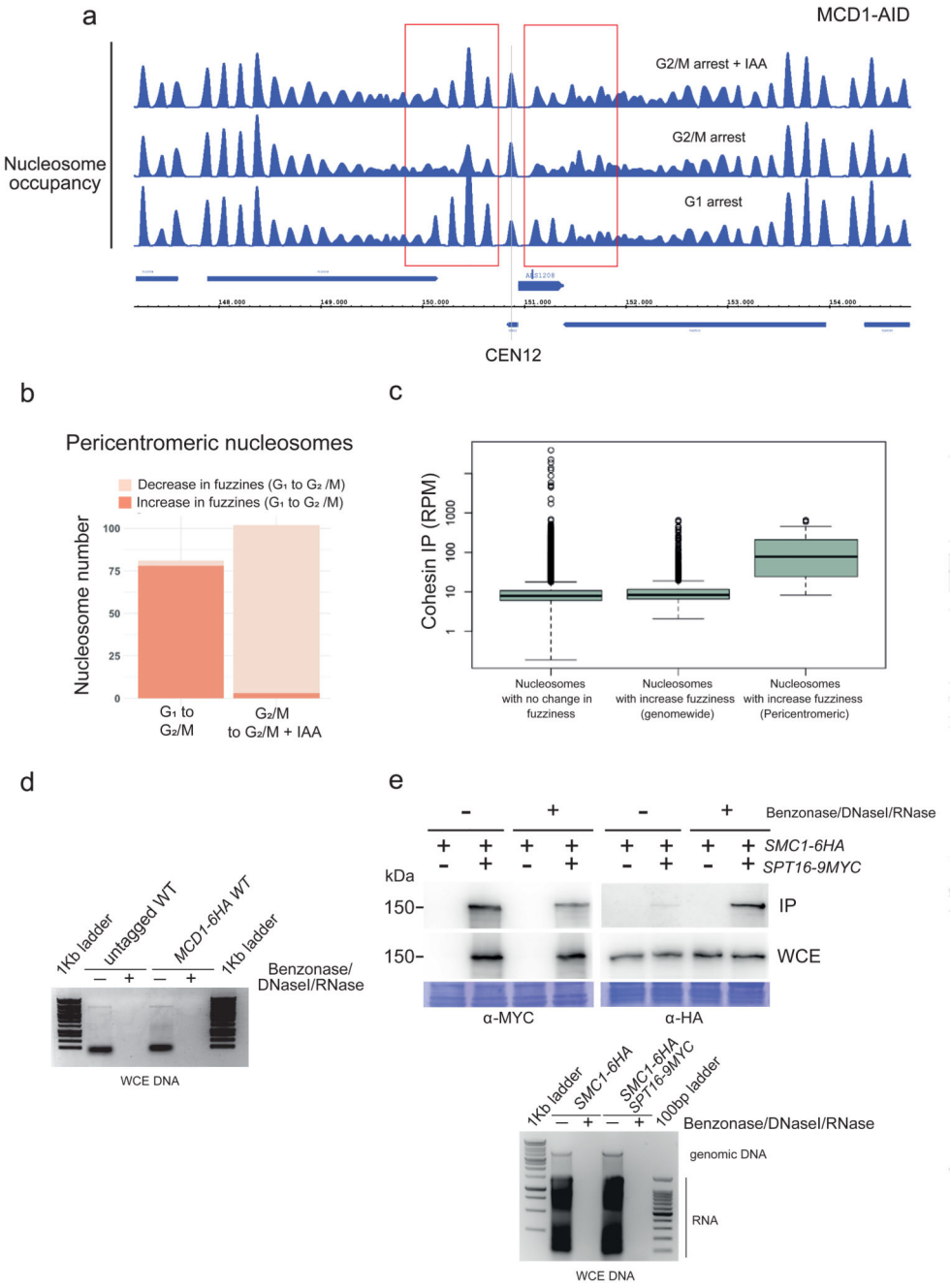

Figure 1. Cohesin complex physically interacts with FACT.

a, Nucleosome occupancy maps of the centromeric region of chromosome 12 in a *S. cerevisiae* strain carrying an auxin degradable allele of Mcd1 (*MCD1-AID*), either arrested in G1 by addition of α–factor (G1 arrest), in metaphase by nocodazole (G2/M arrest), or after auxin-mediated degradation of Mcd1 following G2/M arrest (G2/M arrest + IAA). Regions with changes in nucleosome occupancy are boxed in red. **b**, Whole genome DANPOS analysis of changes in nucleosome fuzziness between G1 and G2/M arrested cells. Y axis represent number of nucleosomes. Bars represent number of nucleosomes that change

Europe PMC Funders Author Manuscripts

fuzziness. Increased fuzziness indicates number of nucleosomes well positioned in G1 that become fuzzy in G2/M, while decrease fuzziness indicates the opposite. From G1 to G2/M, 78 pericentromeric nucleosomes increase fuzziness and 3 decrease fuzziness. In cells arrested in G2/M and treated with IAA to degrade Mcd1-aid 99 pericentromeric nucleosomes decrease fuzziness and 3 increase fuzziness **c**, Box plot of cohesin enrichment with respect to nucleosome fuzziness genome-wide or at pericentromeric regions. Y axis represent log-scale cohesin enrichment in RPM. Box plot of centromeric nucleosomes is focus on pericentric regions (+/- 10kbp of CEN sequences). Centre lines depict the medians; box limits indicate 25th and 75th percentile. The whiskers extend up to 1.5 times the interquartile range from the top (bottom) of the box. The data points beyond that distance are represented as 'outliers'. The differences between the top and bottom whiskers are based on the fact that log transformation of the data does not maintain the distance of a point from the third or first quartile. Y-axis represents cohesin enrichment in RPM at a total of 68841 nucleosomes exhibiting no change in fuzziness, 1393 nucleosomes with increased fuzziness (genomewide) and 78 nucleosomes with increased fuzziness (pericentromeric). **d**, Agarose gel of whole cell extract (WCE) DNA of the pulldown. Cell extracts used for the pulldown were treated with benzonase to eliminate DNA prior to Mcd1 immunoprecipitation, to rule out indirect interactions mediated by DNA. **e**, Immunoprecipitation of Spt16-9myc via the MYC epitope. Smc1-6HA and Spt16-9myc were detected in the pulldowns (IP) and whole cell extracts (WCE) using anti-myc and anti-HA antibodies as indicated. Immunoprecipitation were carried out in the absence and presence of DNaseI/Benzonase/ RNase treatment to remove DNA before the immunoprecipitation. Coomassie stained membranes of the WCE are shown as loading control (top). Agarose gel of whole cell extract (WCE) DNA is shown (bottom). Uncropped blot and gel images are shown in Supplementary Data Set 1. Source data for panels b and c are available online.

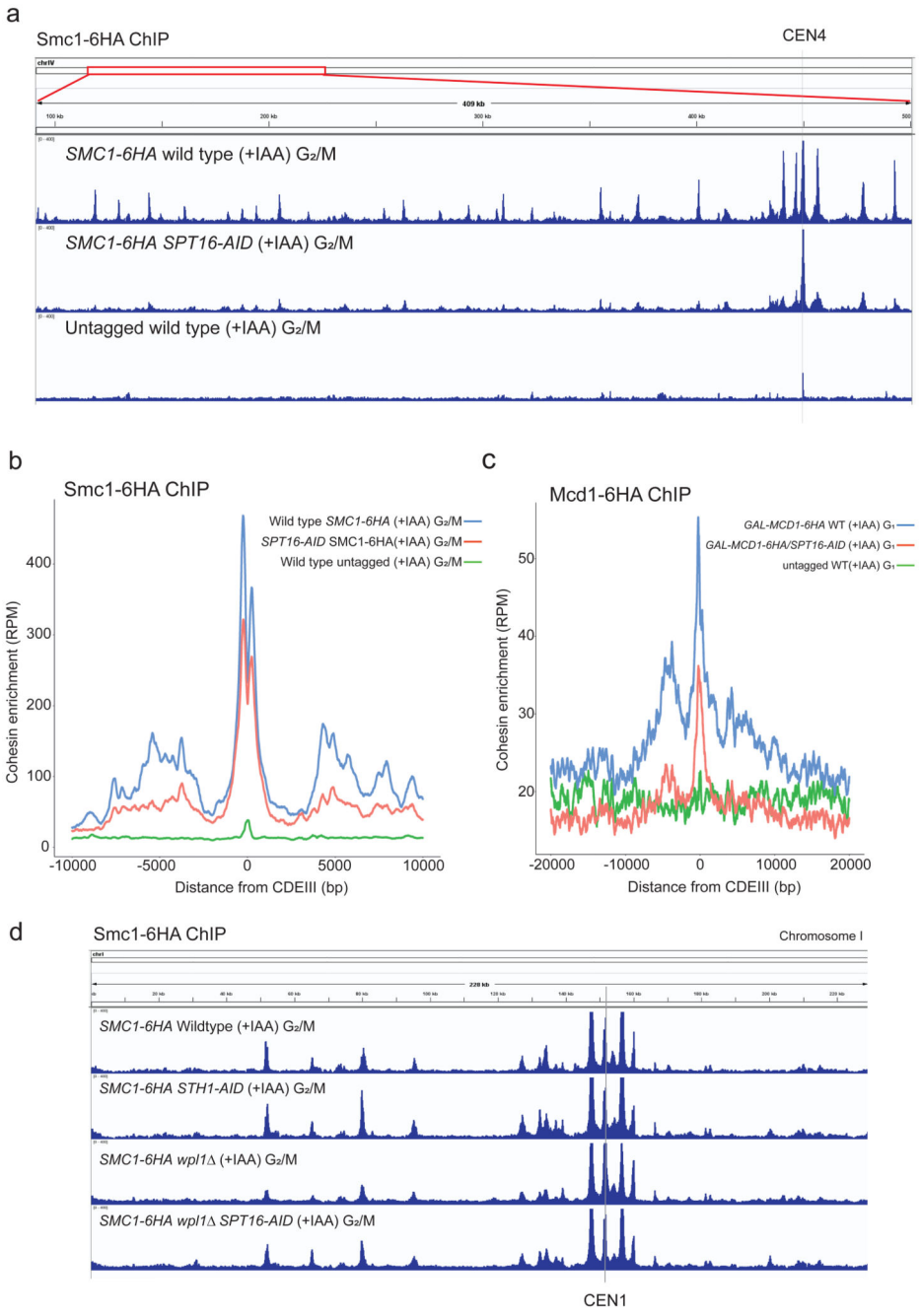

Figure 2. FACT is necessary for the localization of cohesins in metaphase chromosomes.

a, Enrichment of the cohesin subunit Smc1 along a 500 Kb region of *S.cerevisiae* chromosome 4 measured by calibrated ChIP-seq in *SMC1-6HA* wild type, *SMC1-6HA SPT16-AID* and untagged wild type strains arrested in G2/M and treated with auxin (+IAA). **b,** Enrichment of the cohesin subunit Smc1 around *CENs* measured by calibrated ChIP-seq. Smc1-6HA ChIP-seq profiles in *S. cerevisiae* of *SMC1-6HA* wild type, *SMC1-6HA SPT16-AID* and untagged wild type strains arrested in G2/M were compared. The number of reads at each base pair from CDEIII was averaged over all 16 chromosomes. **c**, Enrichment of the

Europe PMC Funders Author Manuscripts

cohesin subunit Mcd1 around *CENs* measured by calibrated ChIP-seq. Average profiles of *MCD1-6HA* of cells arrested in G1 (α–factor) overexpressing *MCD1* from the galactose promoter and treated with auxin (+IAA), in the presence or absence of Spt16 (*SPT16-AID*). The number of reads at each base pair from CDEIII was averaged over all 16 chromosomes. **d,** Enrichment of the cohesin subunit Smc1 along 220 Kb region of *S. cerevisiae* chromosome I measured by calibrated ChIP-seq in *SMC1-6HA* wild type, *SMC1-6HA STH1-AID*, *SMC1-6HA wpl1Δ* or *SMC1-6HA wpl1Δ SPT16-AID* arrested in G2/M and exposed to auxin (+IAA) as denoted.

Europe PMC Funders Author Manuscripts

Europe PMC Funders Author Manuscripts

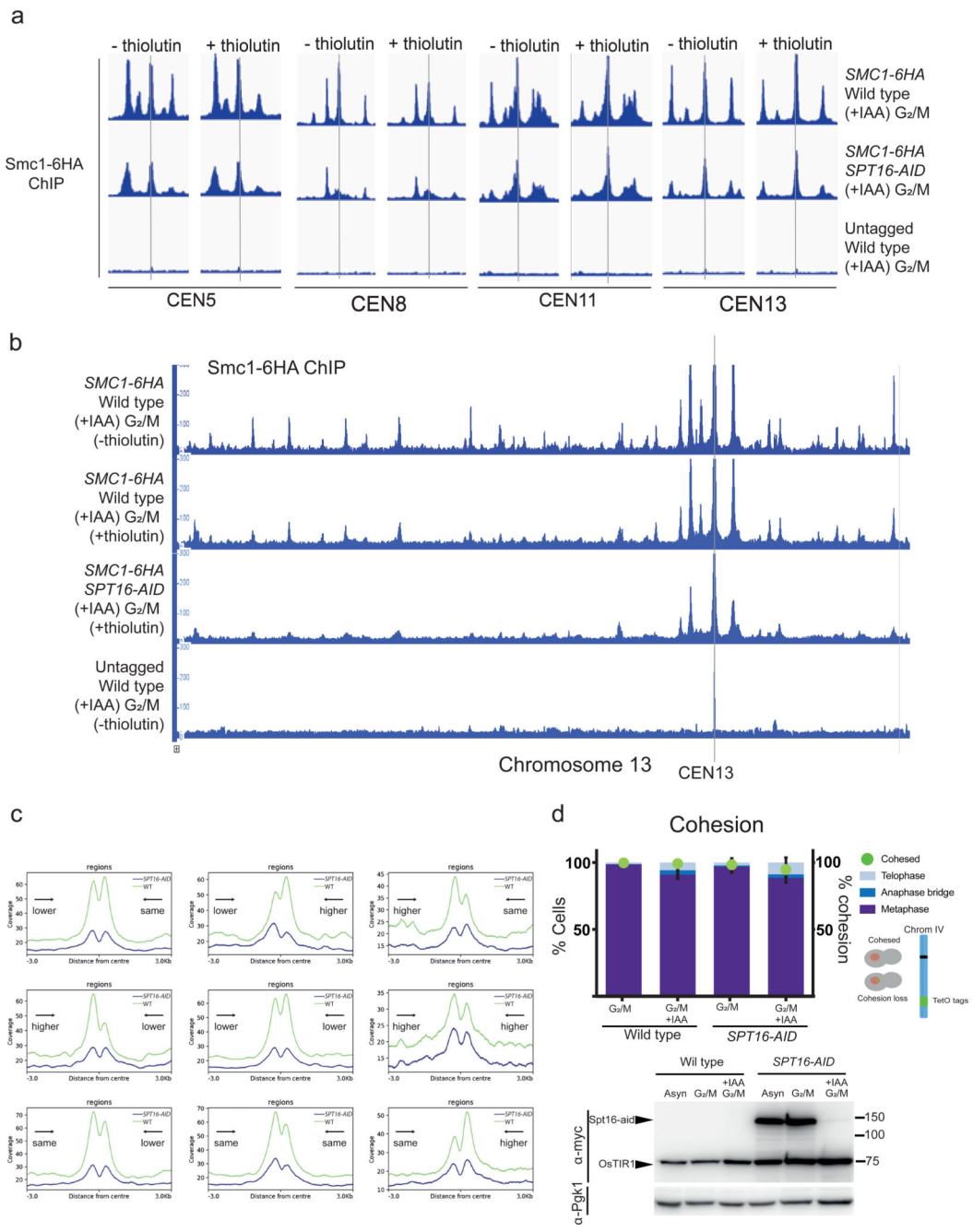

Figure 3. FACT inactivation causes defects in chromosome organisation but not sister chromatid cohesion

a, Enrichment of the cohesin subunit Smc1 around *CEN5*, *CEN8*, *CEN11* and *CEN13* of *S. cerevisiae* measured by calibrated ChIP-seq in *SMC1-6HA* wild type, *SMC1-6HA SPT16-AID* or untagged wild type arrested in G2/M and exposed to auxin in the presence (+) and absence (-) of the transcription inhibitor thiolutin. **b,** Enrichment of the cohesin subunit Smc1 measured by calibrated ChIP-seq on chromosome 13 in *S. cerevisiae* strains *SMC1-6HA* wild type, *SMC1-6HA SPT16-AID* and untagged wild type arrested in G2/M

Europe PMC Funders Author Manuscripts

exposed to auxin as indicated (+IAA) in the presence (+) and absence (-) of the transcription inhibitor thiolutin. **c,** Density profiles of Smc1 binding at convergent gene sites in *SMC1-6HA*, *SMC1-6HA SPT16* strains. Cells were arrested in G2/M with nocodazole and exposed to auxin. Convergent gene sites were subdivided according to transcriptional activity changes (lower, same, higher) upon Spt16 depletion. **d,** Analysis of sister chromatid cohesion in the absence of FACT. Wild type and *SPT16-AID* cells were arrested in metaphase and exposed to auxin to degrade Spt16-aid. (Top) Cell cycle arrest and cohesion analysis. The strains carried *tetO/tetR* based chromosome tags inserted at the right subtelomeric region of chromosome IV, which were used to score loss of cohesion. Bar graphs shows the mean and s.d. of three independent experiments. At least 100 cells were scored per sample and experiment. (Bottom) Western blots of whole cell extracts of wildtype and *SPT16-AID-MYC* strains carrying the *tetO* tag system. Spt16-aid is visualized by α-myc, OsTIR1 was also tagged with myc and is indicated. PGK1 was used as a loading control. Uncropped blot and gel images are shown in Supplementary Data Set 1. Source data for panel d are available online.

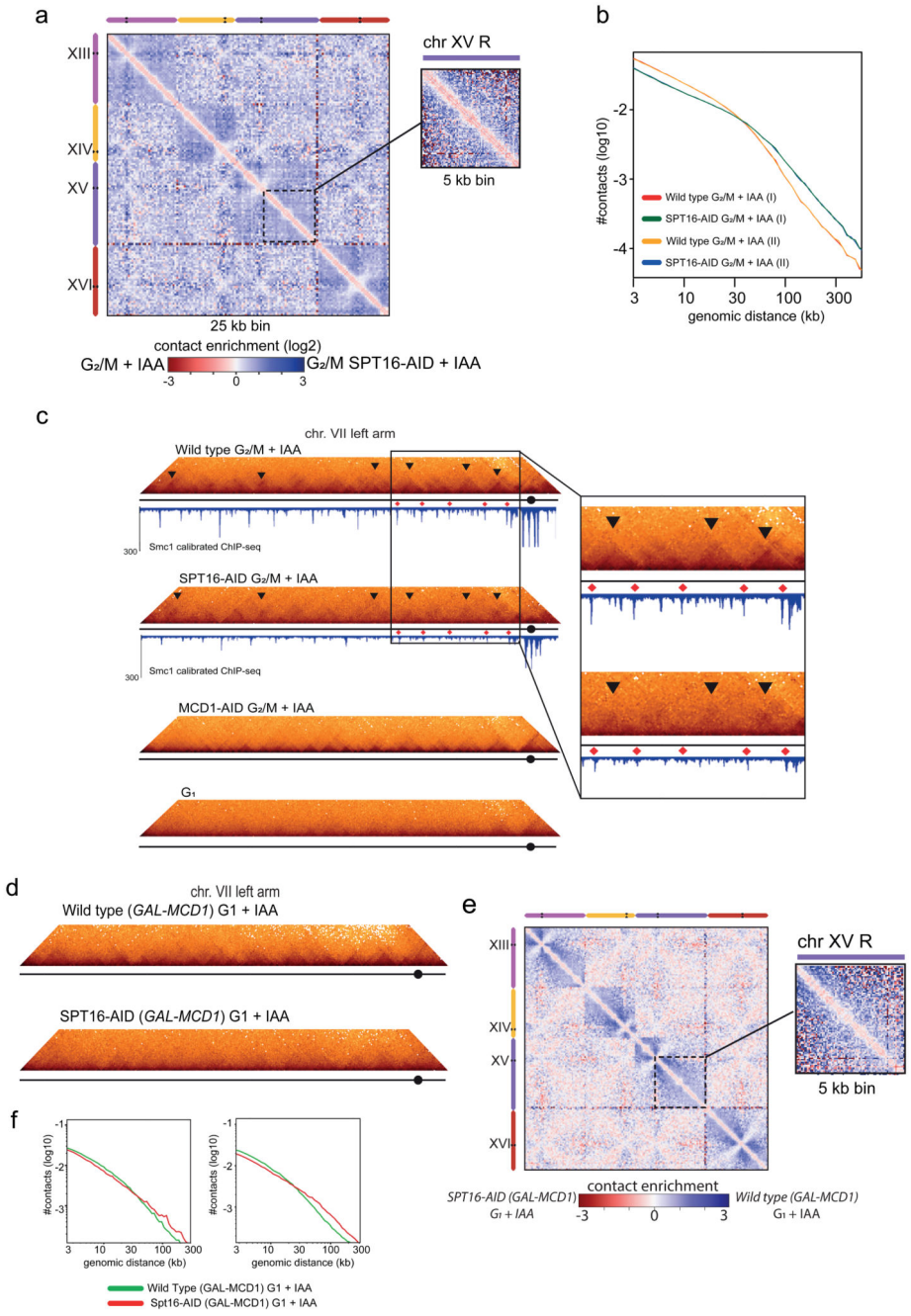

Figure 4. FACT function is important for the establishment cohesin-dependent TAD-like domains

a, Log_2 ratio of the normalized contact map (25 kb bins) of Spt16-aid vs. wild-type metaphase arrested cells treated with auxin. Blue to red color scales reflect the enrichment in contacts observed in wild-type versus Spt16-aid strains, respectively. Inset display magnifications of chr15 at 5 kb resolution. **b,** Contact probability (P(s)) for wild-type and Spt16-aid cells arrested in metaphase averaged over all chromosomes. **c,** Normalized contact maps (at 2kb resolution) of the left arm of chromosome VII of wild type G_1 and G_2/M

Europe PMC Funders Author Manuscripts

arrested cells in the presence of auxin as indicated (+IAA). Spt16 (*SPT16-AID* G_2/M+IAA) or Mcd1 (*MCD1-AID* G_2/M+IAA) were depleted by auxin treatment. The plot underneath the contact map represents enrichment in cohesin as quantified by calibrated ChIP-seq. Black triangles point at TAD-like signals that are lost upon Stp16 depletion. Red diamonds indicate enrichment peaks between TAD-like signals that are lost upon Spt16 depletion. Inset displays higher magnifications of chr7 pericentromeric regions at sites of cohesin (red diamons) and TAD-like domain (black triangles) loss in Spt16 depleted cells compared to control G_2/M arrested cells. **d,** Normalized contact maps (2 kb bins) of the left arm of chromosome VII of G_1 arrested cells overexpressing *MCD1* from the galactose promoter in the presence (Wild type *GAL-MCD1* G_1+IAA) or absence (*SPT16-AID GAL-MCD1* G_1+IAA) of Spt16. **e,** Log_2 ratio of the normalized contact map (25 kb bins) of G1 arrested cells overexpressing MCD1 in the presence and absence of Spt16 as defined above. Blue to red color scales reflect the enrichment in contacts of wild-type versus Spt16-depleted cells, respectively. Inset display magnifications of chr15 at 5 kb resolution. **f,** Contact probability (P(s)) for G_1 arrested cells overexpressing *MCD1* in the presence (Wild type *GAL-MCD1* G_1+IAA) and absence (*SPT16-AID GAL-MCD1* G_1+IAA) of Spt16. Results from duplicate experiments are shown.

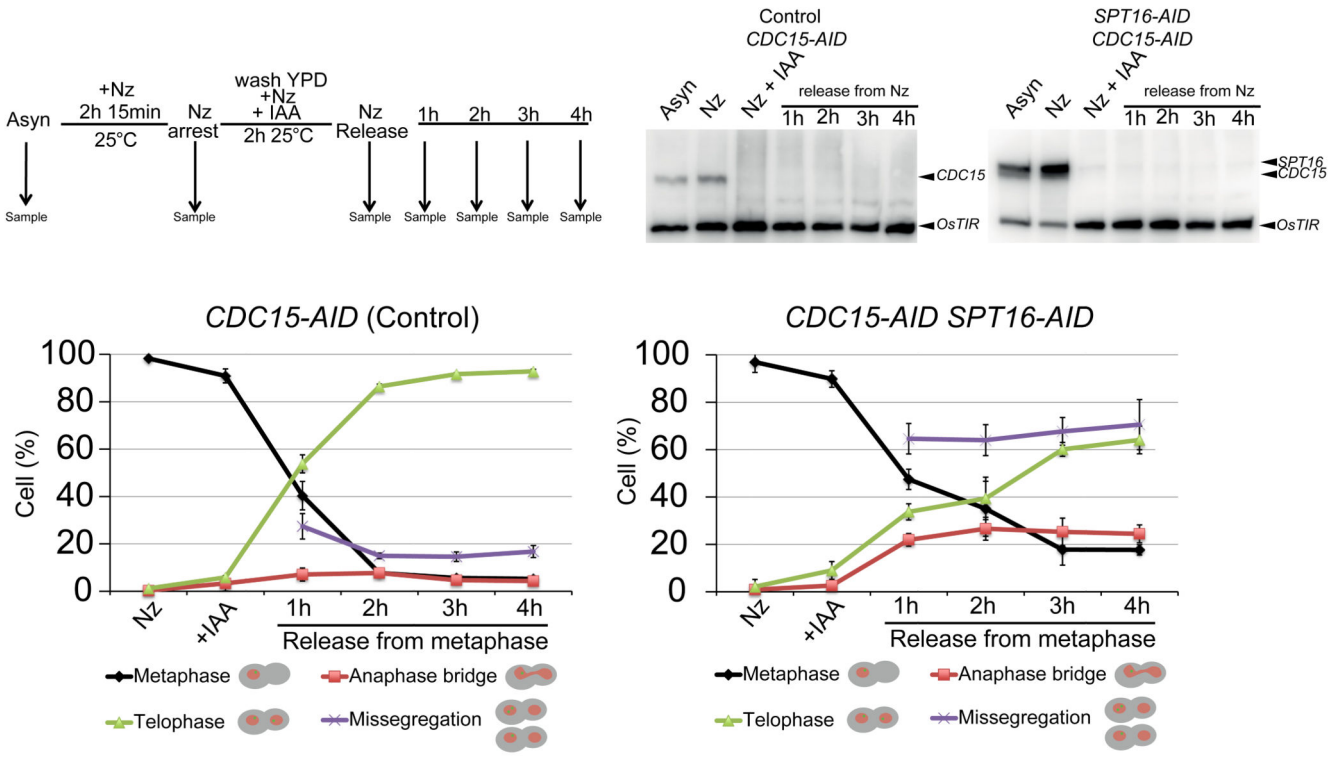

Figure 5. Analysis of chromosome segregation in the absence of FACT.

(Top left) Diagram of the experimental set up. *CDC15-AID* and *CDC15-AID SPT16-AID* cells were arrested in metaphase by nocodazole (Nz) and exposed to auxin (IAA) to degrade Cdc15 and Spt16 and then released from the metaphase arrest into a telophase block caused by the absence of Cdc15. (Top right) Western blots of whole cell extracts from *CDCD15-AID-MYC* and *CDC15-AID-MYC SPT16-AID-MYC* strains, blotted with a α-myc antibody. OsTIR1 was also tagged with myc and it is indicated. (Bottom) Graphs show cell cycle stage and chromosome segregation after Nocodazole release in *CDC15-AID* and *CDC15-AID SPT16-AID* strains. Chromosome segregation was tracked using tetO/tetR-based chromosome tags inserted at right subtelomere region of chromosome IV. The mean and s.d. of three independent experiments are shown. At least 100 cells were scored per sample and experiment. Uncropped blot images are shown in Supplementary Data Set 1. Source data for the graphs are available online.

Europe PMC Funders Author Manuscripts

Europe PMC Funders Author Manuscripts

Table 1

Summary of cohesin subunits and chromatin remodelers interacting with HA-tagged *MCD1*, including enrichment values and the number of peptides identified. Asterisks in the enrichment column represent proteins identified in the tagged but not in the wild type untagged control elution.

Gene	Protein ID	Log2 fold change pE/nE	Razor + unique
SMC3	P47035	8.09	58
SMC1	P32908	7.73	54
SPT16	P32558	4.38	19
STH1	P32597	2.92	15
IRR1	P40541	*	31
MCD1	Q12158	*	29
CHD1	P32657	*	16
PDS5	Q04264	*	14
RSC8	P43609	*	3
EAF3	Q12432	*	3
SWI1	P09547	*	2
RSC1	P53236	*	2
RSC9	Q03124	*	3
RSC3	Q06639	*	3
MSI1	P13712	*	2
POB3	Q04636	*	2